Energy Conversion Systems: Molecular Architecture Engineering of Metal Precursors and their Applications to Vapor Phase and Solution Routes

Journal:	*Journal of Materials Research*
Manuscript ID	JMR-2020-0509
Manuscript Type:	Invited Feature Paper - REVIEW
Date Submitted by the Author:	03-Jul-2020
Complete List of Authors:	Pellegrino, Anna; Università degli Studi di Catania, Scienze Chimiche Lucchini, Giacomo; Università degli Studi di Verona, Dipartimento di Biotecnologie Speghini, Adolfo; Università degli Studi di Verona, Dipartimento di Biotecnologie Malandrino, Graziella; Università degli Studi di Catania, Scienze Chimiche
Key Words:	chemical vapor deposition (CVD) (deposition), sol-gel, film

SCHOLARONE™
Manuscripts

Energy Conversion Systems: Molecular Architecture Engineering of Metal Precursors and their Applications to Vapor Phase and Solution Routes

Anna Lucia Pellegrino,[1] Giacomo Lucchini[2], Adolfo Speghini,[2] Graziella Malandrino,[1,*]

1.Dipartimento di Scienze Chimiche, Università di Catania and INSTM UdR Catania V.le A. Doria 6, 95125 Catania Italy. E-mail: gmalandrino@unict.it

2. Nanomaterials Research Group, Dipartimento di Biotecnologie, Università di Verona and INSTM UdR Verona, Strada le Grazie 15, 37134 Verona, Italy. E-mail: adolfo.speghini@univr.it

For Peer Review

ABSTRACT

A careful engineering of the central metal coordination spheres provides adducts with excellent properties for application as precursors in vapor phase and solution processes. The family of precursors under study concerns the fluorinated metalorganic β-diketonates of alkaline, alkaline-earth and rare-earth metals adducted with a polyether, with general formula $M(hfa)_n \cdot L$ (M= Ca, Na, Y, Yb, Er, Tm; Hhfa = 1,1,1,5,5,5 hexafluoroacetylacetone, L= diglyme or tetraglyme). Mass transport properties, such as volatility and thermal stability, of these adducts have been deeply analyzed through thermogravimetric analysis and differential scanning calorimetric measurements. These properties are rationalized in relation to the metal coordination sphere in the precursors and their applications. In particular, the precursors under focus have been applied to Metal Organic Chemical Vapor Deposition (MOCVD) and a combined sol-gel/spin-coating approach. Both methods allow to obtain selectively and reproducibly CaF_2 and $NaYF_4$ phases with several combinations of lanthanide doping ions, using a proper mixture of fluorinated precursors. A careful optimization of both synthetic strategies is the key point for the production of different lanthanide doped binary and multicomponent fluoride films, i.e. CaF_2: Yb^{3+},Er^{3+}, CaF_2: Yb^{3+},Tm^{3+}, CaF_2: Yb^{3+},Er^{3+},Tm^{3+} and $NaYF_4$: Yb^{3+},Er^{3+}, $NaYF_4$: Yb^{3+},Tm^{3+}, with suitable morphologies, compositions and crystalline structures. The films show very promising upconversion properties,

thus pointing to their appealing applications in photovoltaic systems and white light emission devices.

I. INTRODUCTION

In the recent scenario of new functional materials for energetic applications, fluoride-based systems represent an emergent class of inorganic materials with application fields ranging from solar cells to phosphors in microelectronics [1-2], from photocatalysis to nano-biomedicine devices [3-4]. Particularly, lanthanide doped fluoride films have been studied for energy conversion applications for their unique luminescent properties under light irradiation [5].

Fluoride systems such as binary CaF_2 and SrF_2 or multicomponent $NaYF_4$ and $NaGdF_4$ have been studied as inorganic host materials with doping luminescent lanthanide ions (Ln^{3+}: Yb, Er, Tm) in form of nanoparticles or compact thin films for energy conversion processes [6-7]. Depending on the active luminescence centers, energy conversion processes take place as upconversion or downconversion and down shifting mechanisms. We focus our attention on upconversion (UC) processes, which involve luminescent mechanisms of active species which adsorb two or more photons in the near infrared region and generate photons with higher energy, usually in the visible or ultraviolet regions. Typically, this phenomenon involves lanthanide doped inorganic materials and occurs through energy transfer processes between a sensitizer species, usually Yb^{3+}, which adsorbs and transfers energy to an active element, such as Er^{3+} or Tm^{3+} [8]. The possibility to design a proper combination of host and active species allows to define the properties of the final functional materials. For instance, Yb^{3+}-Er^{3+} or Yb^{3+}-Tm^{3+} doped fluoride materials have raised increasing interest in photovoltaic technology for enhancement of solar cell efficiency through UC mechanisms, responsible of increasing the portion of the solar spectrum useful for the solar device [9]. A proper combination of doping ions, i.e. Yb^{3+}, Er^{3+} and Tm^{3+} percentages, are also of interest for producing white light emission through mixing of red, green, and blue emissions of Er^{3+} and

For Peer Review

Tm^{3+} ions [10]. In addition, the direct correlation between luminescence emission spectra and temperature has been used for the production of nano-thermometer useful as microelectronic mapping system in the integrated circuits [11].

The host lattice nature is a crucial issue for an efficient UC process and, among binary and multicomponent fluorides, CaF_2 and $NaYF_4$ are the most promising candidates for efficient UC systems [12]. In fact, they show high optical transparency in the UV to IR range, high chemical stability, and low phonon energies, which minimize non radiative de-excitation processes. A comment deserves the $NaYF_4$ host, which is stable as cubic (α) or hexagonal (β) phases. Several studies have demonstrated that the hexagonal β-$NaYF_4$ phase is a better host lattice for energy conversion applications [13]. Thus, synthetic approaches with high selectivity for the production of the pure β-$NaYF_4$ phase are highly recommended. Furthermore, the massive application of these materials in photovoltaic devices requires their fabrication in form of thin films with industrial appealing methodologies.

Among the vapor phase routes, Metal Organic Chemical Vapor Deposition (MOCVD) method [14] represents a well-established industrial technique applied for thin film production of oxide-based semiconductor devices and for Si-based solar cell fabrication. Particularly, in the field of fluoride-based energy conversion systems, the possibility to improve the solar module performance, just adding an extra layer of UC material in the same production lines, represents one of the main advantages of this approach. In fact, the MOCVD process is a reliable and reproducible method for the fast production of thin films over large areas with a high uniformity degree in both morphology and composition. In this context, several fluorinated β-diketonate precursors have been successfully applied for the MOCVD production of pure and lanthanide doped oxide and fluoride systems [15,16].

At the same time, the sol-gel method has been successfully applied for fluoride thin film production by exploiting the excellent solubility and reactivity of the fluorinated precursors. The

For Peer Review

sol-gel process, combined with spin-coating or spraying depositions, has the advantages of a low-cost approach with the possibility of tuning the doping percentages, and a great potential for scaling up.

For both synthetic approaches, the development of multifunctional precursors through suitable synthetic methodologies are crucial for their massive applications.

In this perspective, the first part of this feature article presents an overview of alkaline, alkaline-and rare-earth metal precursors of the type $M(\beta\text{-diket})_n \cdot L$ [β-diket = Hhfa = 1,1,1,5,5,5 hexafluoroacetylacetone, $L=CH_3O(CH_2CH_2O)_nCH_3$ with n=2 diglyme (bis(2-methoxyethyl)ether), and n=4 tetraglyme (2,5,8,11,14-pentaoxapentadecane)], with a particular focus on $Na(hfa)\bullet$tetraglyme, $Ca(hfa)_2\bullet$diglyme$\bullet H_2O$ and $M(hfa)_3\bullet$diglyme (M = Y, Yb, Er, Tm) adducts, known as "second-generation" precursors [16-19]. The accurate engineering of the central metal coordination spheres through the use of the polyether species, i.e. diglyme and tetraglyme, and fluorinated β-diketonate hfa ligands allows the design of stable precursors, useful for MOCVD, or high soluble and cleanly decomposable precursors useful for the sol-gel process. The complex structures have been obtained through single crystal X-ray diffraction and their thermal stability, volatility and mass transport properties have been deeply studied through termogravimetric analysis (TGA) and differential scanning calorimetric (DSC) measurements. Structural properties of the adducts and the choice of polyether ligands, strictly related to the ionic radius and charge of the central metal ions, influence their thermal properties and transport characteristics, matching in each case the vapor phase and/or the solution synthetic applications.

To the best of our knowledge, the $M(hfa)_n\bullet$glyme family complexes represent one of the best precursor classes for MOCVD processes and are widely studied and applied for the fabrication of transition metal oxides, lanthanide-based phases, and fluoride materials [20-22]. Furthermore, for fluoride thin film fabrication, the presence of fluorine in the precursor structures provides a source of fluorine, thus avoiding the use of external sources, such as HF reagent.

For Peer Review

In the second part of this feature article, the focus is on the development of synthetic strategies for the fluoride thin film production using the above mentioned alkaline, alkaline-earth and rare-earth metal precursors $M(hfa)_n \cdot L$ through vapor phase routes and solution approaches [19, 23-25]. The $Ca(hfa)_2 \bullet diglyme \bullet H_2O$ and $Ln(hfa)_3 \bullet diglyme$ have been successfully applied in MOCVD processes for the fabrication of CaF_2:Yb(18%),Er(2%), CaF_2:Yb(18%),Tm(2%), and CaF_2:Yb(18%),Er(2%),Tm(1%) thin films. Furthermore, a sol-gel/spin-coating deposition process has been applied for their synthesis as well. An accurate optimization of the two different methods has been the key point for the production of homogeneous and compact doped CaF_2 coatings showing energy conversion properties. Analogously, a sol-gel methodology has been successfully developed for the production of $NaYF_4$:Yb(18%),Er(2%) and $NaYF_4$:Yb(18%),Tm(0.5%) thin films starting from $Na(hfa) \bullet tetraglyme$, $Y(hfa)_3 \bullet diglyme$ and $Ln(hfa)_3 \bullet diglyme$ (Ln = Yb, Er, Tm) precursors. An in-depth luminescent characterization has proven the upconversion properties of the different layers.

II. OVERVIEW OF ALKALINE, ALKALINE-EARTH AND RARE-EARTH METAL PRECURSORS

The key points for the metal precursors synthesis and massive use for thin film productions are their stability and their mass transport properties. The chemical stability of a metalorganic adduct is a sum of different aspects and is the first issue to address, in order to provide monomeric and thermally stable metal source.

Among a plethora of precursor architectures, we focus our attention on alkaline, alkaline- and rare-earth metal precursors of the type $M(\beta\text{-diket})_n \cdot L$, known as “second-generation” precursors [26-29], made by the combined use of fluorinated β-diketonate ligands and ancillary coordinated polyether species. The $M(\beta\text{-diket})_n \cdot L$ complex can be synthesized through one-pot reactions in organic solvents by mixing metal oxides, hydroxides, or acetates and β-diketonate ligands, such as

For Peer Review

the hexafluoroacetylacetone, and polyether ligands, i.e. monoglyme, diglyme, triglyme or tetraglyme [16-19].

A. How to engineer molecular architectures?

Mainly, engineering of the final metalorganic complex reflects at first instance the intrinsic nature of the central metal in terms of ionic radius and oxidation state. The most stable oxidation state for rare-earth metals is +3, and for elements close to $4f^0$, $4f^7$ or $4f^{14}$ configurations also the +2 and +4 oxidation states can be stabilized, such as for Eu, Yb and Ce, Pr, respectively. The ionic radii of the Ln^{3+} follow the typical lanthanide contraction behavior from La^{3+} to Lu^{3+} (varying from 1.16 Å to 0.98 Å for an eight-coordination number [30]), as a consequence of the incomplete shielding of the nucleus by 4f electrons and due to the direct effect of the atomic number increasing from 57 to 71 [31]. As a result of these intrinsic properties, the Ln^{3+} ions are stabilized in high coordination numbers, usually greater than 6 and often up to 9–10. The rare-earth Y^{3+} ion has a behavior similar to the heavier lanthanide species due to the similar ionic radius (1.02 Å for an eight-coordination number [30]). Alkaline metal complexes, instead, are commonly observed in lower coordination numbers from 6 to 8, and usually stable in octahedral coordination. In the case of the alkaline-earth metals, coordination numbers up to 11 have been observed in the case of the large barium metal center [32].

Relationship coordination spheres-thermal properties – The saturation of the inner coordination sphere is the main point to engineer molecular architectures and consequently to tailor precursor properties. Particularly, the choice of the ligands allows a fine balance between stability and reactivity needed for their use in thin film fabrications. The previous “first-generation” rare-earth element precursors, such as $M(tmhd)_3$ (Htmhd = 2,2,6,6-tetramethyl-3,5-heptanedione), have shown some disadvantages due to the poor volatility and stability to atmosphere [33]. In fact, they usually tend either to polymerize or to react with nucleophilic impurities such as donor solvents, producing low volatile multiple complex species [34]. These drawbacks have been overcome by

For Peer Review

modeling new molecular architectures, in which the coordination sphere is saturated by polyether Lewis bases, thus competing with oligomerization and hydration side reactions, and achieving steric saturation of the metal center [16,35].

A comment deserves the case of $Ca(hfa)_2$•diglyme•H_2O, widely discussed below, which is an excellent candidate for both vapor and solution approaches, despite the water molecule coordination. The excellent mass transport properties, in terms of thermal stability and high volatility of the calcium complex, are, in fact, mainly related to its monomeric form and to the saturation of the inner sphere in a stable eight-fold coordination.

It is worth to note that also the choice of the polyether length is crucial for the molecular engineering. For instance, the $La(hfa)_3$•polyether series has been deeply studied as a function of different polyethers, i.e. monoglyme, diglyme, triglyme and tetraglyme [17]. If on one hand, the monoglyme ligand allows the coordination of one water molecule to complete the coordination sphere of the lanthanum ion, on the other hand, with the longer tetraglyme, only four of the five oxygen atoms of the glyme are involved in the coordination. For these reasons, the most stable and applied complex for La^{3+} and also for the slightly smaller Y^{3+}, Er^{3+}, Tm^{3+} and Yb^{3+} is the $M(hfa)_3$•diglyme structure with a nine-coordination architecture.

Mass transport properties and thermal behavior **-** The design of the precursors' architectures has a direct effect on the mass transport properties of the complexes to produce suitable thin film precursors. Thermogravimetric and differential scanning calorimetry analyses provide the first screening tests for the mass transport properties of these adducts. These analyses provide useful information on the thermal stability, mass transport properties and the eventual presence of a decomposition processes during the vaporization step.

The "second-generation" adducts represent one of the most thermally stable and highly volatile class of precursors for vapor route synthetic approaches. The presence of fluorinated ligands, in fact, avoids the formation of H bonds between molecules and provides a less packed structure in

For Peer Review

the lattice. In addition, the electron withdrawing effect of the fluorine atoms increases the net positive charge on the metal ion and, as a consequence, the complex is stabilized due to hard–hard interactions with the polyether species. Particularly, it has been widely demonstrated that the fluorinated ligands enhance the reactivity of the molecules and confer them excellent thermal stability and volatility properties [16]. However, these fluorinated precursors may suffer of problems related to the incorporation of undesired fluorine contaminants in the film and they often stabilize oxyfluoride and/or fluoride phases. This drawback becomes, in contrast, one of the main advantages of these metal precursors for the fabrication of energy conversion materials, being the fluoride phases among the most efficient matrices. Furthermore, the fluorinated metal precursors avoid the use of the external fluorine source. On the other hand, an accurate control of operative conditions allows to overcome this effect in the case of phase film thermodynamically more stable than the fluoride phase, e.g. rare-earth based perovskite films [36]. In the case of metal transition based thin film materials the thermodynamic stabilization of the oxide phases and the oxidative condition stabilize the formation of pure oxide phases, as reported for the NiO thin film synthesis from the $Ni(hfa)_2$tmeda (tmeda = N,N,N',N'-tetramethylethylenediamine) adduct [20].

For Peer Review

B. **Case studies of precursors' structures**

In this section, we present in details the structures and thermal behaviors of the $Ca(hfa)_2$•diglyme•H_2O, Na(hfa)•tetraglyme and $M(hfa)_3$•diglyme (M =Y, Yb, Tm, Er) precursors, which have been tested for the fabrication of pure and Ln doped CaF_2 and β-$NaYF_4$ thin films.

$Ca(hfa)_2$•diglyme•H_2O **-** The $Ca(hfa)_2$•diglyme•H_2O single crystal structure has been determined by X-ray diffraction and deeply studied for the first time by Kuzmina et al. [37]. The crystalline complex consists of mononuclear molecules in which the Ca cation is located in a distorted anti-prismatical coordination formed by four O atoms of the two hfa anions, three O of the diglyme

molecule, and one O from a water molecule [Fig. 1(a)]. Notably, the thermal characterization demonstrated that sequential dehydration and vaporization processes occur either in argon or air atmosphere. The vaporization step is a quantitative process at temperature up to 200 °C with a weight loss of about 97% [38]. The present fluorinated Ca complex, therefore, represents a suitable candidate for vapor phase route and it has been tested as a single source precursor for the MOCVD synthesis of CaF_2 thin films. The first report of its application by Makarevich et al. [39] shows the water assisted MOCVD synthesis of epitaxial CaF_2 thin films on (001) $SrTiO_3$ substrates. The presence of water in this specific case increased the deposition rate and reduced the activation energy of the film deposition process at temperature below 500°C. The growth of epitaxial CaF_2 films is related to their use in the technological field of superconducting material and microelectronic devices.

Recently, using the same fluorinated calcium precursor, $Ca(hfa)_2$•diglyme•H_2O, we have optimized an innovative MOCVD process, in which at lower temperature of 400°C, binary and ternary lanthanides doped CaF_2 thin films have been obtained on silicon and glass substrates [23,24]. For the first time, also the solution approach has been successfully tested for the synthesis of Ln doped CaF_2 thin films [23]. Both methods represent industrially appealing and easily scalable processes to produce energy conversion materials, and the possibility to mix different fluorinated β-diketonates, such as the $Ca(hfa)_2$•diglyme•H_2O and $Ln(hfa)_3$•diglyme (Ln = Yb, Tm, Er) compounds, represents the key issue of the innovative use of these fluorinated precursors.

$Ln(hfa)_3$•diglyme (Ln = Y, Yb, Tm, Er)- The single crystal structure of this class of compounds are quite similar to the one observed for the $La(hfa)_3$•diglyme [17]. The formation of nine coordinated complexes is showed in Fig. 1(b) in which the metal center is coordinated by six O atoms of the three hfa ligands and three O of the diglyme, with a total coordination number of nine.

Therefore, the complete saturation of the metal sphere avoids the coordination of nucleophilic species such as H_2O molecules.

For Peer Review

Figure 1

The thermal characterization of $Yb(hfa)_3$•diglyme, $Tm(hfa)_3$•diglyme and $Er(hfa)_3$•diglyme, presented in Fig. 2, is characterized by excellent mass transport properties and quantitative vaporization processes with a single step loss and residues less than 2% in weight. Additionally, $Ln(hfa)_3$•diglyme (Ln = Yb, Tm, Er) precursors present high solubility in common organic solvents and a good reactivity in solution processes. For these reasons, they have been widely used both in MOCVD and sol-gel processes.

Figure 2

Particularly, $Y(hfa)_3$•diglyme has been tested for the production of ternary lanthanide fluoride materials, i.e. $NaYF_4$ thin films, using a sol-gel approach. Mixtures of Yb, Er and Tm adducts, in various stoichiometric ratios, have been used as well, as multi component sources of lanthanide doping ions both in MOCVD and sol-gel processes [19,25].

Na(hfa)•tetraglyme - The fluorinated β-diketonate adduct Na(hfa)•tetraglyme, recently reported, has been successfully used as sodium precursor with $Ln(hfa)_3$•diglyme (Ln = Y, Yb, Er, Tm) complexes in the sol-gel synthesis of Ln-doped β-$NaYF_4$ thin films [19,25]. The Na(hfa)•tetraglyme structure in Fig. 1(c) presents the central metal coordinated by the two O atoms of the hfa ligand and by the five O of the tetraglyme, with a total coordination number of seven.

However, the thermal behavior of the complex, shown in the TG curve [Fig. 3(a)], points to a decomposition process in the range of 130-250°C. In fact, the residue of about 9.8% suggests the loss of the ligands during the heating process and may be associated with the formation of the NaF byproduct. The differential scanning calorimetric data in Fig. 3(b) shows two endothermic peaks: the first at 43 °C, likely associated with a solid-solid transition, and the second at 67 °C due to the

For Peer Review

adduct melting. The final peak at around 240 °C may be correlated to exothermic processes associated with the ligand loss. Nevertheless, the sodium precursor shows a good reactivity in solution and high solubility in common organic solvents, such as dichloromethane, acetone and ethanol. For these reasons, it represents a proper candidate for sodium based thin films through solution approaches. In fact, the complex has been tested in equimolar mixture with the $Y(hfa)_3$•diglyme adduct for the synthesis of $NaYF_4$ pure phase and of doped $NaYF_4$: Er^{3+}, Yb^{3+} and Tm^{3+}, Yb^{3+} using a proper amount of $Ln(hfa)_3$•diglyme (Ln = Yb, Er, Tm) complexes. The complex mixture acts as a single source of metals and fluorine and an accurate optimization of the operative parameters allows to obtain selectively and reproducibly the pure phase β-$NaYF_4$ in form of compact thin films.

Figure 3.

C. Precursors' thermal properties vs. applications to film growth

Therefore, thermal stability, volatility and solubility are the main parameters to select the precursors which fit the required properties for the vapor or solution methodologies. An overview of the precursors' main characteristics and their uses are summarized in the Scheme 1. The majority of the fluorinated β-diketonate complexes, such as the $M(hfa)_3$•diglyme series with M = La, Y, Yb, Tm, Er, etc., are widely used as precursors for thermal MOCVD method. They show, in fact, high volatility and excellent thermal stability, with a unique vaporization step and a final residue lower than 4% in weight, which represent the perfect match for vapor phase approaches. Additionally, if the complexes show solubility and stability in the most common organic solvents, they can be good candidates for liquid assisted MOCVD approach as well. Metalorganic complexes, which show significant reactivity behavior in vapor phase, may be applied for atomic layer deposition. Clearly, the solution approach requires high degree of solubility and reactivity in

For Peer Review

addition to the characteristics explained above. Particularly, Na(hfa)•tetraglyme, $Ca(hfa)_2$•diglyme•H_2O and $Ln(hfa)_3$•diglyme precursors have been successfully tested for the sol-gel/spin-coating approach to the synthesis of doped fluoride thin films.

Scheme 1

Thermal behavior of precursors mixture- Interestingly, the mass transport properties of the $Ca(hfa)_2$•diglyme•H_2O and $Ln(hfa)_3$•diglyme precursors have been studied also as mixture for both MOCVD and sol-gel/spin-coating thin film approaches.

The fabrication of energy conversion material requires an accurate tailoring of the luminescence species amount and thus, the possibility to easily adjust the composition of the final layer, just changing the composition and the stoichiometry of the starting mixture, is an important issue.

Particularly, the precursors used for the fabrication of CaF_2: Yb, Er ; CaF_2:Yb,Tm and CaF_2:Yb,Tm, Er thin films have been characterized through dynamic thermogravimetric (TG) measurements. The TG curves in Fig. 2 display the thermal behavior of the single precursors and a mixture of 80% $Ca(hfa)_2$•diglyme•H_2O and 20% of $Yb(hfa)_3$•diglyme, which represents the maximum amount of doping ions, usually present in an efficient energy conversion Ln-doped systems. Reasonably, we suppose that, having $Er(hfa)_3$•diglyme and $Tm(hfa)_3$•diglyme complexes TG curves comparable to the analogous Yb complex, the mixtures containing also small amounts of Er and Tm have a similar thermal behavior of the Ca-Yb mixture. The TG curve of the Ca-Yb precursor mixture shows a single step weight loss in the range of 170-220°C with a similar behavior of the single complexes and a residue of about 2 %. This behavior clearly points to a single source performance with a unique vaporization step for the two precursors. Notably, a single vaporization step does not involve the same reactivity of the two components, which can have different decomposition rates during the vapor deposition process [23]. However, the presence of the same ligands in the Ca and

For Peer Review

Ln adducts could be one of the main reasons of this unique performance. In fact, the ligand exchange process may be excluded in this case and the mixture behavior, in terms of thermal stability and volatility, is similar to those of the single complexes. For these reasons, the Ca-Yb precursor mixture has been deeply studied and used for MOCVD approach and sol-gel process as well.

II. SYNTHETIC STRATEGIES FOR FLUORIDE FILM DEPOSITIONS

A. Binary fluoride: Ln-doped CaF_2 thin film

MOCVD approach **-** MOCVD method has been successfully applied to the fabrication of Ln-doped CaF_2: Yb,Er, CaF_2:Yb,Tm and CaF_2:Yb,Er,Tm thin films on Si, quartz, and glass substrates, starting from the β-diketonate $Ca(hfa)_2$•diglyme•H_2O and $Ln(hfa)_3$•diglyme (Ln = Tm, Er, Yb) compounds. Indeed, the above discussed thermal precursor characteristics allow to use mixtures of Ca and Ln compounds as a multicomponent precursor, modulating the doping ion composition of the final films and thus their functional properties. Furthermore, the $Ca(hfa)_2$•diglyme•H_2O adduct acts as a single-source precursor for calcium and fluorine.

An in-depth study was conducted on the correlation between the lanthanide molar ratio in the multicomponent starting mixture and the percentages found in the final films through energy dispersive X-ray analysis (EDX) analysis [23]. This study confirms that an appropriate tuning of the Ca-Ln starting mixture composition, at a specific deposition temperature, allows to tailor the final doping of the films and, in turn, their luminescence properties.

Phase crystallinity studies, conducted in function of doping ion amounts and deposition temperatures, have shown that undoped CaF_2 thin films deposited on Si (100) in the 400-550 °C range exhibit patterns [Fig. 4(a)] associated with the formation of pure cubic CaF_2 phase (ICDD card n.35-0816) due to the presence of characteristic peaks at 28.24°, 47.02° and 55.74° related to

For Peer Review

111, 220 and 311 reflections, respectively. Independently from the deposition temperature, the pure CaF_2 phase is detected without any preferential orientation.

In order to study the effect of the doping ion composition in the CaF_2 lattice, several CaF_2 thin films were prepared using different lanthanide combination in terms of ion nature (Yb, Er and Yb, Er, Tm) and doping percentages (Ln doping = 7-38%). The *a*-axis parameters have been calculated, using graphite as an internal standard, through the relationship between hkl and lattice parameter for a cubic structure and the comparison of the *a* values of the doped CaF_2 thin films has been summarized in Table 1. A closer look to the patterns in the range of the 220 peaks [Fig. 4(b)] shows a shift toward higher angles for all the CaF_2: Yb,Er thin films with a total amount of Ln ions up to 23% . On the contrary, an inversion of this tendency is observed for CaF_2 samples with Ln ions amount of 28% and 38%.

Figure 4

Considering that Ca^{2+} and Ln^{3+} ions in an 8-fold coordination present similar ionic radii (Ca^{2+}: 1.12 Å vs. Yb^{3+}:0.985 Å, Er^{3+}: 1.004 Å and Tm^{3+}:0.994 Å [30]), it is likely that the lanthanide ions are incorporated in the lattice as substitutional species for Ca^{2+} ions. As a direct consequence, the *a*-axis parameter variation, in function of the doping percentage, has been rationalized considering a balance between two different contributions: (i) the slight smaller ionic radii of Ln species compared to Ca^{2+} and their substitution to Ca^{2+} positions in the lattice, and (ii) the effects of charge compensation occurring in the structures due to insertion of fluoride ions or clusters. The first contribution causes a lattice contraction and thus a shift of the diffraction peaks towards higher 2-theta values. This effect is predominant for low doped systems, i.e. CaF_2: Er,Yb with %Er+Yb of 7%, 18% and 23%, and results in a contraction of the *a*-axis parameter from 5.46 to 5.44 Å. On the contrary, the second effect is predominant for high doping systems, i.e. CaF_2:Er,Yb,Tm

For Peer Review

with %Er+Yb+Tm of 28% and 38%, and it acts in an opposite way causing an increase of *a*-axis values from 5.46 to 5.47 Å. Despite the small distortions of the lattice due to the doping ions, both systems CaF_2:Er,Yb and CaF_2:Yb, Er, Tm show high luminescence signals and represent excellent candidates for upconversion properties.

Table 1. Values of the *a*-axis parameters for the undoped and Ln^{3+} doped CaF_2 thin films grown on Si in the range 400-500 °C.

MOCVD APPROACH				
Composition	**T_{dep} (°C)**	**Average doping of all the Ln^{3+} * (%)**	**a-axis (Å)**	**Ref.**
CaF_2	—	—	5.4630	ICDD 35-0816
CaF_2	500	Undoped	5.46(02)	[24]
CaF_2: Yb, Er	500	7	5.45(3)	[24]
CaF_2: Yb, Er	500	18	5.44(6)	[24]
CaF_2: Yb, Er	500	23	5.44(5)	[24]
CaF_2:Yb,Er,Tm	400	28	5.47(6)	[23]
CaF_2:Yb,Er,Tm	450	38	5.47(7)	[23]
*determined by EDX				

The field emission scanning electron microscopy (FE-SEM) analysis has allowed to study the effects of substrate nature and doping ions on the film morphologies, confirming the homogeneity of the CaF_2 deposits in the range of 400-550 °C deposition temperature. However, all the deposition processes of CaF_2 thin films deposited on Si substrates require slow cooling rate (3°C/min) from deposition temperature to room temperature, due to the different thermal expansion coefficient of CaF_2 and Si, which cause cracking and swelling effects on the deposited surfaces [24]. The CaF_2:Yb^{3+}(18%), Er^{3+}(2%) films deposited on Si have a very homogeneous and smooth surface [Fig. 5(a)]. Despite the slow cooling process from 500 °C to 25 °C, some cracking is still barely visible. The CaF_2:Yb^{3+}(18%), Er^{3+}(2%) films deposited on quartz have very compact surface with larger and regular crystalline grains of about 150 nm [Fig. 5(b)]. The analogous CaF_2:Yb^{3+}(18%), Tm^{3+}(2%) films

[Fig. 5(c)] show a similar morphology with grains of about 200 nm. Finally, the tridoped systems CaF_2:Yb^{3+}(18%), Er^{3+}(2%), Tm^{3+}(1%) on glass presents crystalline and compact surfaces with grains of about 100 nm [Fig. 5(d)]. The slight changing of the morphologies observed in these samples may be related to the different effect of doping ion concentration and substrate nature on the nucleation and growth process of the CaF_2 films.

Figure 5.

Sol-gel/spin-coating approach - $Ca(hfa)_2$•diglyme•H_2O complex has been successfully applied for the sol-gel synthesis of CaF_2 thin films on different substrates as well. Appropriate mixture of $Ca(hfa)_2$•diglyme•H_2O and $Ln(hfa)_3$•diglyme (Ln = Yb, Tm, Er) compounds have been tested for the production of UC systems, using the suitable percentage of doping ions. The sol has been prepared in ethanol solution under acid catalysis using the optimized conditions reported in ref. 23.

The final annealing treatment at 350 °C or 400 °C yields crystalline and compact CaF_2 thin films. Notably, the samples have been obtained after annealing treatment that are up to 150°C lower than those recently reported [40].

X-ray diffraction (XRD) patterns collected on samples grown on different substrates, i.e. Si and glass, confirm the formation of pure single phase CaF_2 independently of the substrate nature. In Fig. 6 the XRD patterns of undoped CaF_2 (red line) and CaF_2:Yb^{3+}(18%),Er^{3+}(2%),Tm^{3+}(1%) (blue line) films, obtained at 400 °C on Si (100), display peaks at 2θ = 28.25°, 47.00°, and 55.75° associated with the 111, 220, and 311 reflections of pure polycrystalline CaF_2 phase (ICDD card n.35-0816). In the inset, a closer look to the 220 peaks underlines the shift at higher angle of the peaks for the doped systems. Thus, analogously to the MOCVD grown CaF_2 films, the *a*-axis parameters of 5.46(04) Å and 5.45(8) Å have been extrapolated for both undoped and doped CaF_2

For Peer Review

samples, respectively. The first parameter is similar to the one reported in the ICCD card for the pure system and it is mainly coincident to the analogous system obtained through MOCVD (5.46(02)Å). This behavior points to the formation of pure CaF_2 phase without any distortion or impurities. The absence of impurities, such as carbon or oxide byproducts, have been checked through EDX analysis as well. Indeed, the *a* parameter of 5.45(8) Å found for the CaF_2:Yb^{3+}(18%),Er^{3+}(2%),Tm^{3+}(1%) thin film is in agreement with the behavior already found for the low doped CaF_2 systems obtained through the MOCVD method (see table 1 for comparison). In fact, also here, we can explain the lattice parameter reduction from 5.4630 Å (value reported on ICDD card n. 35-0816) to 5.45(8) Å (for CaF_2:Yb^{3+}(18%),Er^{3+}(2%),Tm^{3+}(1%) thin film), considering the substitution of lanthanide ions at the Ca^{2+} sites, thus causing a contraction of the lattice due to their slight smaller ionic radii compared to Ca^{2+} species.

Figure 6

The homogeneity of the CaF_2:Yb^{3+}(18%),Er^{3+}(2%),Tm^{3+}(1%) thin film has been evaluated through EDX map analyses on the surface (Fig. 7). The erbium and thulium elements have not been collected due to their low amounts, which are at the detectability limit of the technique. Their presence is instead confirmed by luminescence measurement, as described below. The EDX analysis displays the formation of compact CaF_2 deposition in the entire surface (Fig. 7 - Ca and F maps) with a very homogeneous distribution of doping Yb ions, which act as the sensitizer element for the UC properties of the final material.

Figure 7

The field emission scanning electron microscopy (FE-SEM) images of the pure and doped CaF_2 films obtained for different annealing temperatures and substrates are reported in Fig. 8. The

For Peer Review

undoped CaF_2 sample deposited at 400 °C on glass displays a homogeneous coating with small grains of the order of about 150 nm and the presence of some cracks [Fig. 8(a)]. This morphology suggests the phenomena of grains coalescence during the formation of the coating, probably due to the annealing treatment. Conversely, under the same deposition conditions, the CaF_2:Yb^{3+}(18%),Er^{3+}(2%)Tm^{3+}(1%) film on Si [Fig. 8(b)] presents a quite different coating, with smaller grains of about 50 nm distributed in a compact way and some barely visible cracks. The cross section in Fig. 8(c) confirms a compact deposit with a thickness of about 750 ± 45 nm. In Fig. 8(d), the analogous CaF_2:Yb^{3+}(18%), Er^{3+}(2%), Tm^{3+}(1%) sample on Si obtained at lower annealing temperature shows a similar morphology.

Therefore, the two temperatures 350-400 °C adopted for the annealing treatment do not significantly affect either the morphology or the phase nature, but only the crystalline characteristics of the films. The nature of the substrate, instead, seems to play an important role on the morphology of the films. The differences in the morphology of the films obtained on Si and on glass may be likely due to the different wettability of the untreated Si and glass substrates.

The comparison between the morphologies of CaF_2 thin films obtained through MOCVD and sol-gel method highlights indeed the strong effect of the synthetic approach, with the formation of more nanostructured deposits for the MOCVD samples and smoother and smaller grains-based deposits for the sol-gel approach.

Figure 8

B. Ternary fluorides: Ln-doped β-$NaYF_4$ thin films

Sol-gel/spin-coating method - Starting from an equimolar Na(hfa)•tetraglyme and $Y(hfa)_3$•diglyme adducts solution, it has been reported the synthesis of pure hexagonal $NaYF_4$ thin films through a sol-gel/spin-coating method. The optimized procedure has been used to obtain the

For Peer Review

doped $NaYF_4$: Yb^{3+}(18%),Er^{3+}(2%) and $NaYF_4$: Yb^{3+}(18%),Tm^{3+}(0.5%) thin films as well, starting from a proper solution of Na(hfa)•tetraglyme and $Ln(hfa)_3$•diglyme (Ln = Y, Yb, Er, Tm) precursors. Details of the sol-gel and spin-coating steps are reported in reference 19,25.

Through an accurate optimization of the operative conditions, such as molar ratio of the adducts, density of the sol and annealing treatment, the complex mixture allowed to obtain selectively and reproducibly the pure β-$NaYF_4$ phase in form of compact thin films. The composition of the films have been checked through EDX analysis on different sites of the deposits and confirm the composition of doped films in agreement with the composition of the starting mixtures, i.e. $NaYF_4$:Yb(18%),Er(2%) and $NaYF_4$:Yb(18%),Tm(0.5%).

The XRD characterizations show the formation of the pure hexagonal phase, which represents the best host lattice for the doping ion luminescence activities compared to the cubic phase. Interestingly, using graphite as an internal standard, the comparison of the XRD patterns in Fig. 9 confirms that the peak positions of the co-doped $NaYF_4$:Yb(18%),Er(2%) and $NaYF_4$:Yb(18%),Tm(0.5%) films correspond perfectly to the peak positions of the undoped phase (ICDD card n. 16-0334). This aspect suggests that the doping ions are substitutional to Y ones in the $NaYF_4$ lattice, thus the Ln^{3+} and Y^{3+} ions are located in the same nine-fold coordination environment. Therefore, the lattice structure does not present any distortion because of the similar ionic radii of the Yb^{3+} (1.042 Å, 9-fold coordination), Tm^{3+}(1.052 Å, 9-fold coordination), Er^{3+} (1.062, 9-fold coordination) , and Y^{3+} (1.075 Å, 9-fold coordination) [30]. Moreover, differently from the doped CaF_2 film cases, the presence of interstitial fluoride ions or clusters may be ruled out, due to the same charge 3+ of Y and Ln species.

Figure 9

For Peer Review

The FE-SEM images of the doped and undoped β-$NaYF_4$ films deposited on Si [Fig. 10 (a-c)] show the formation of homogeneous and uniform films over large areas (1 × 2 cm) with a porous and quite flat surfaces. The pure β-$NaYF_4$ and the doped β-$NaYF_4$:Yb(18%),Er(2%) films present rounded grains of about 250 nm and 200 nm, respectively [Fig. 10(a,b)]. In Fig. 10(c), the doped $NaYF_4$:Yb(18%),Tm(0.5%) film on Si has a similar porous surface with less regular grains, with dimensions ranging from 200 to 300 nm. The analogous thin film obtained on quartz substrate [Fig. 10(d)] presents instead a more porous and irregular surface.

Figure 10

Therefore, the doping species do not affect widely the final film morphology, while the substrate nature has a strong effect on the final morphology of the films, probably due to the different wettability of the Si and quartz substrates.

III. TOWARDS EFFICIENT ENERGY CONVERSION DEVICES IN THE OPTICAL SPECTRAL REGION

A. Upconversion emission of lanthanide doped CaF_2 thin films

Upconversion is a process in which two or more photon of a radiation in a spectral region (usually the optical spectral region) are absorbed by a suitable material and then an emission radiation at higher energies (Anti-Stokes process) is generated [41-44]. This phenomenon is particularly interesting if the exciting radiation has energy in the near infrared region, since emission radiation in the UV or visible region is generated. This behavior is of paramount importance for materials that can be considered of interest as energy converters in solar cell devices [45,46]. Lanthanide doped oxide or fluoride based materials are among the most efficient upconverters, for their low phonon energies and therefore low non-radiative decay probabilities of the excited states of the emitting ions [47]. Typical excitation radiation for generating UC radiation in the visible and UV

For Peer Review

regions has a wavelength of 980 nm, in the near infrared region. The experimental setup and details of measurements for all the upconversion results are reported in the ref. 23.

Bright emission was shown by a nanostructured Tm^{3+}, Yb^{3+} ions doped CaF_2 thin film, prepared by MOCVD, under 980 nm laser excitation [Fig. 11(a)]. The spectra show several bands due to Tm^{3+} ions in the UV, visible and near infrared region (NIR) spectral regions. Tm^{3+} ion transitions are assigned (Fig. 11 (a)] as in the following to (1) $^1D_2 \rightarrow {}^3H_6$; (2) $^1D_2 \rightarrow {}^3F_4$; (3) $^1G_4 \rightarrow {}^3H_6$, (4) $^1D_2 \rightarrow {}^3H_5$, (5) $^1G_4 \rightarrow {}^3F_4$, (6) $^1G_4 \rightarrow {}^3H_5$, (7) $^3H_4 \rightarrow {}^3H_6$. While the strongest band is around 460-480 nm, in the blue region, other emission bands are observed, spread in all the optical region. A red band is visible, around 650 nm, as well as a band in the near infrared region, in the range 750-850 nm. Similarly, a nanostructured Er^{3+}, Yb^{3+} doped CaF_2 thin film shows very bright luminescence under 980 nm laser excitation as it can be appreciated in Fig. 11(b). Er^{3+} ion transitions are assigned to (8) $^2H_{1/2} \rightarrow {}^4I_{15/2}$, (9) $^4S_{3/2} \rightarrow {}^4I_{15/2}$, (10) $^4F_{9/2} \rightarrow {}^4I_{15/2}$ [Fig. 11(b)]. In this case, a green (at 525-550 nm) and red emission (around 660 nm) is clearly observed, due to radiative transitions of the Er^{3+} ions, sensitized by the Yb^{3+} ions after absorption of photons at 980 nm. The red emission is slightly stronger than the green one, as noted by the relative intensities of the ($^2H_{11/2}$, $^4S_{3/2}$) $\rightarrow {}^4I_{15/2}$ transitions with respect to the $^4F_{9/2} \rightarrow {}^4I_{15/2}$ one. In the case of the tridoped film, typical emission bands due to Er^{3+} ions and Tm^{3+} ions in the visible and NIR are found [Fig. 11(C)].

Figure 11.

A scheme of the several energy transfer processes and radiative emissions in Yb^{3+}, Er^{3+} and Yb^{3+}, Tm^{3+} codoped systems are shown in Fig. 12. These experimental evidences clearly indicate that an efficient $Yb^{3+} \rightarrow Er^{3+}$ or Tm^{3+} energy transfer is present for both the Yb^{3+}, Er^{3+} and Yb^{3+}, Tm^{3+} codoped CaF_2 thin film samples.

For Peer Review

Many photon absorption steps can be involved in the generation of the upconversion emission, not only in the near infrared and visible regions, but also in the UV region, after population of very high energy levels, as shown in Fig. 12. In fact, particularly interesting are the emission bands in the UV region, around 360 nm, for the Tm^{3+} ions, as evidenced in Fig. 11(a). Although less efficient than the emission band in the visible and near infrared regions, the upconversion in the UV region can be very useful and can be considered to trigger chemical reactions that need high energy photons to occur. As an example, photocatalytic reactions are particularly interesting to consider as upconverted radiation can allow photodegradation of pollutants under near infrared illumination, possibly also solar driven [47-49].

Figure 12.

It is also interesting to investigate the color properties of the upconversion emission of the various lanthanide codoped CaF_2 based thin films. For this aspect, a chromaticity coordinate analysis was carried out, important tool to understand how the human eye will perceive the color of a certain emission. This analysis considers the response of the cones of the retina of the human eye to a light in the Red, Green and Blue (RGB) ranges and the color coordinates are plotted in the so-called CIE 1931 space. The obtained color coordinates for the analyzed samples are shown in Fig. 13. Importantly, we have to point out that slight variations of the CIE coordinates for the lanthanide emissions could be observed by varying the power density of the exciting laser radiation.

In our cases, the emissions of the Er^{3+}, Yb^{3+} ions codoped thin films (for both the CaF_2 and $NaYF_4$ hosts, see below) are in the yellow region and using a power density of 3.2 W/mm^2 the CIE 1931 coordinates are x=0.40, y=0.53. On the other hand, the Tm^{3+}, Yb^{3+} ions codoped thin film emission is in the blue region, due to the relevant emission band of Tm^{3+} ions around 460 nm and using a

For Peer Review

power density of 3.2 W/mm^2 the CIE 1931 coordinates are x=0.17 and y=0.19 (see Fig. 13). On the other hand, the tridoped Er^{3+}, Tm^{3+}, Yb^{3+} ions thin film shows an almost perfectly white emission upon laser excitation at 980 nm (using a power density of 1 W/cm^2) with CIE 1931 coordinates of x=0.35, y=0.39. The white colour is due to the emission contributions of both the Er^{3+} and Tm^{3+} ions, since they emit in different color regions.

Figure 13.

B. Upconversion emission of Ln doped $NaYF_4$ thin films

A similar upconversion behavior has been observed for Er^{3+}, Yb^{3+} and Tm^{3+}, Yb^{3+} codoped hexagonal $NaYF_4$ based thin films. In particular, in Fig. 14 spectra of these samples are shown, upon excitation at 980 nm. The observed bands are typical of the lanthanide ions and similar to those found for the lanthanide doped CaF_2 based thin films, shown in Fig. 12. Thus, Tm^{3+} ion transitions are assigned [Fig. 14 (a)] as in the following to (1) $^1D_2 \rightarrow {}^3H_6$; (2) $^1D_2 \rightarrow {}^3F_4$; (3) $^1G_4 \rightarrow {}^3H_6$, (4) $^1D_2 \rightarrow {}^3H_5$, (5) $^1G_4 \rightarrow {}^3F_4$, (6) $^1G_4 \rightarrow {}^3H_5$, (7) $^3H_4 \rightarrow {}^3H_6$, while Er^{3+} ion transitions are assigned to (8) $^2H_{1/2} \rightarrow {}^4I_{15/2}$, (9) $^4S_{3/2} \rightarrow {}^4I_{15/2}$, (10) $^4F_{9/2} \rightarrow {}^4I_{15/2}$ [Fig. 14(b)].

Figure 14

The CIE coordinates for the two $NaYF_4$ samples, shown in Fig. 13, are also similar to those found for the lanthanide doped CaF_2 thin films. It should be remarked that the β-$NaYF_4$ structure is one of the most interesting crystal structures for hosting luminescent lanthanide ions. This is also due to the very high upconversion efficiency found for lanthanide doped β-$NaYF_4$ as recently evidenced by some authors [44,50,51]. Although measurements of quantum efficiency for upconversion emission for thin film could be laborious [52], an estimate of the upconversion

For Peer Review

efficiency or at least a comparison among the upconversion properties of different thin films constituted by various hosts would be of paramount importance to find the best conditions for efficient emissions.

For this reason, it would be very valuable to continue a careful investigation on thin films of lanthanide doped β-$NaYF_4$, also prepared with different experimental techniques as MOCVD and sol-gel methods, that could permit to tune the conditions for optimal luminescence efficiency.

IV SUMMARY

This feature article gives an overview of the intricate balance between metal precursor architecture, with general formula $M(hfa)_n$•glyme, and their properties in terms of mass transport and chemical reactivity. An accurate engineering of the metal coordination sphere allows to tailor precursor properties for application in vapor phase or solution routes.

These two different synthetic approaches have been explored to fabricate lanthanide doped calcium fluoride and sodium yttrium tetrafluoride thin films with upconversion properties. A comparison between vapor phase and solution routes has been discussed in function of deposition temperature, doping ions and substrate nature, using the same starting reagents, i.e. β-diketonate glyme adducts. Both approaches represent challenging methods for the synthesis of fluoride based matrices starting from fluorinated metal precursors, which act efficiently as single sources for metal and fluorine. MOCVD has the advantage to be a fast and easily scalable process, already industrially applied in the photovoltaic panel production. On the other hand, the sol–gel process, if combined with a spraying deposition procedure, would have the advantage of being a low cost approach with a great potential for scaling up. In relation to luminescence properties of these doped materials, the power studies indicate that the upconversion emission can be generated with relatively low laser power densities, pointing to very good upconversion efficiencies for both the sol–gel/spin-coated and MOCVD prepared films.

For Peer Review

In our opinion, given the great advantages of both techniques, that permit to easily tune the conditions for optimal luminescence efficiency, future applications of both routes can be envisaged to fabricate fluoride films for other energy conversion devices, such as downshifting and downconverter systems, and for white light emitting materials.

ACKNOWLEDGMENTS

The authors thank the University of Catania for financial support within the "Piano della Ricerca di Ateneo 2016–2018" and the University of Verona for funding in the framework of the project “Joint Projects 2018”. A. L. P. and G. M. thank Bionanotech Research and Innovation Tower (BRIT) laboratory of University of Catania for the diffractometer facility.

For Peer Review

REFERENCES:

[1] **D. Ma, Y. Shen, T. Su, J. Zhao, N. Ur Rahman, Z. Xie, F. Shi, S. Zheng, Y. Zhang, Z. Chi:** Performance enhancement in up-conversion nanoparticle-embedded perovskite solar cells by harvesting near-infrared sunlight. *Mater. Chem. Front.* **10**, 2058-2065 (2019).

[2] **J. Du, Y. An, C. Zhang, C. Zhu, X. Li, D. Ma:** Photonic Design and Electrical Evaluation of Dual-Functional Solar Cells for Energy Conversion and Display Applications. *Nanoscale Res. Lett.* **14**, 1-9 (2019).

[3] **H. Kwon, F. Marques Mota, K. Chung, Y. J. Jang, J. K. Hyun, J. Lee, D. H. Kim:** Enhancing Solar Light-Driven Photocatalytic Activity of Mesoporous Carbon-TiO2 Hybrid Films via Upconversion Coupling. *ACS Sustain. Chem. Eng*. **6**, 1310-1317 (2018).

[4] **M. Zhang, M. Zuo, C. Wang, Z. Li, Q. Cheng, J. Huang, Z. Wang, Z. Liu:** Monitoring Neuroinflammation with an HOCl-Activatable and Blood–Brain Barrier Permeable Upconversion Nanoprobe. *Anal. Chem.* **92**, 5569-5576 (2020).

[5] **L. Liang, D. B. L Teh, N. D. Dinh, W. Chen, Q. Chen, Y. Wu, S. Chowdhury, A. Yamanaka, T. C. Sum, C. H. Chen**: Upconversion amplification through dielectric superlensing modulation *Nat. Commun.* **10**,1-9 (2019).

[6] **A. A. Lyapin, P. A. Ryabochkina, S. V. Gushchin, M. N. Zharkov, A. S. Ermakov, V. M. Kyashkin, S. V. Prytkov, A. V. Atanova**: Characteristics of Upconversion Luminescence of CaF_2:Er Powders Excited by 1.5-μm Laser Radiation. *Opt. Spectrosc.* **128**, 200–206(2020).

[7] **Q. Zhao, J. Zhao, M. Tao, C. Wang, X. Zeng, Y. Hu, S. Wang, M. Zeng, W. Zhou, H. Gu, Y. Li:** Controllable planar electrodeposition of $NaYF_4$: Yb^{3+}, Er^{3+} thin films with efficient upconverting fluorescence. *J. Lumin.* **214**, 116580/1-7 (2019).

[8] **M. Kaczmarek:** Lanthanide-sensitized luminescence and chemiluminescence in the systems containing most often used medicines: a review. *J. Lumin.* **222**, 117174/1-22 (2020).

[9] **D. Lu, C. Mao, S. K. Cho, S. Ahn, W. Park**: Experimental demonstration of plasmon enhanced energy transfer ratein $NaYF_4$:Yb^{3+},Er^{3+} upconversion nanoparticles. *Sci. Rep.* **6**, 18894/1-11 (2016).

[10] **C. Cao, W.Qin, J. Zhang, Y. Wang, G. Wang, G. Wei, P. Zhu, L. Wang, L. Jin**: Up-conversion white light of Tm^{3+}/Er^{3+}/Yb^{3+} tri-doped CaF_2 phosphors. *Opt. Commun.* **281**, 1716–1719 (2008).

[11] **Y. Hao, S. Lv, Z. Ma, J. Qiu:** Understanding differences in Er^{3+}–Yb^{3+} codoped glass and glass ceramic based on upconversion luminescence for optical thermometry. *RSC Adv.* **8**, 12165-12172 (2018).

[12] **S. Fischer, R. D. Mehlenbacher, A. Lay, C. Siefe, A. P. Alivisatos, J. A. Dionne**: Small Alkaline-Earth-based Core/Shell Nanoparticles for Efficient Upconversion. *Nano Letters* **19**, 3878-3885 (2019).

[13] V**. N. K. B. Adusumalli, H. V. S. R. M. Koppisetti, S. Ganguli, S. Sarkar and V. Mahalingam**: Tuning the Energy Transfer Efficiency between Ce^{3+} and Ln^{3+} Ions (Ln=Tm, Sm, Tb, Dy) by Controlling the Crystal Phase of $NaYF_4$ Nanocrystals, *Chem. – Eur. J.* **23**, 994–1000 (2017).

For Peer Review

[14] **M. L. Hitchman, K. F. Jensen**: Chemical Vapor Deposition: Principles and Applications, Academic Press, London, (1993).

[15] **M. R. Catalano, G. Cucinotta, E. Schiliro, M. Mannini, A. Caneschi, R. Lo Nigro, E. Smecca, G. G. Condorelli, G. Malandrino:** Metal-Organic Chemical Vapor Deposition (MOCVD) Synthesis of Heteroepitaxial $Pr_{0.7}Ca_{0.3}MnO_3$ Films: Effects of Processing Conditions on Structural/Morphological and Functional Properties. *ChemistryOpen* **4,** 523-532 (2015).

[16] **G. Malandrino, I. L. Fragalà:** Lanthanide "second-generation" precursors for MOCVD applications: Effects of the metal ionic radius and polyether length on coordination spheres and mass-transport properties. *Coord. Chem. Rev.* **250,** 1605-1620 (2006).

[17] **G. Malandrino, C. Benelli, F. Castelli, I. L. Fragalà:** Synthesis, Characterization, Crystal Structure and Mass Transport Properties of Lanthanum β-Diketonate Glyme Complexes, Volatile Precursors for Metal−Organic Chemical Vapor Deposition Applications. *Chem. Mater.* **10**, 3434-3444 (1998).

[18] **G. Malandrino, I. L. Fragalà, S. Aime, W. Dastrù, R. Gobetto, C. Benelli:** Synthesis, crystal structure and solid-state dynamics of the $La(hfa)_3{\cdot}Me(OCH_2CH_2)_4OMe$ (Hhfa = 1,1,1,5,5,5-hexafluoropentane-2,4-dione) precursor for MOCVD applications. *J. Chem. Soc. Dalton Trans.* **9,** 1509-1512 (1998).

[19] **M. R. Catalano, A. L. Pellegrino, P. Rossi, P. Paoli, P. Cortelletti, M. Pedroni, A. Speghini, G. Malandrino:** Upconverting Er^{3+}, Yb^{3+} activated β-$NaYF_4$ thin films: a solution route using a novel sodium β-diketonate polyether adduct. *New J. Chem.* **41**, 4771-4776 (2017).

[20] **S. Battiato, M. M. Giangregorio, M. R. Catalano, R. Lo Nigro, M. Losurdo, G. Malandrino:** Morphology-controlled synthesis of NiO films: the role of the precursor and the effect of the substrate nature on the films' structural/optical properties. *RSC Adv.* **6**, 30813-30823 (2016).

For Peer Review

[21] **G. Malandrino, L. M. S. Perdicaro, I. L. Fragalà**: Effects of processing parameters in the MOCVD growth of nanostructured lanthanum trifluoride and oxyfluoride thin films. *Chem. Vap. Deposition* **12**, 736-741 (2006).

[22] **M. E. Fragala, R. G. Toro, S. Privitera, G. Malandrino**: MOCVD fabrication of magnesium fluoride films: Effects of deposition parameters on structure and morphology. *Chem. Vap. Deposition* **17**, 80-87 (2011).

[23] **A. L. Pellegrino, S. La Manna, A. Bartasyte, P.Cortelletti, G.Lucchini, A. Speghini, G. Malandrino:** Upconverting tri-doped calcium fluoride-based thin films: a comparison of the MOCVD and sol–gel preparation methods. *J. Mater. Chem. C* **8**, 3865-3877 (2020).

[24] **A. L. Pellegrino, P. Cortelletti, M. Pedroni, A. Speghini, G. Malandrino**: Nanostructured CaF_2:Ln^{3+} (Ln^{3+} = Yb^{3+}/Er^{3+}, Yb^{3+}/Tm^{3+}) Thin Films: MOCVD Fabrication and Their Upconversion Properties. *Adv. Mater. Interfaces* **4**, 1700245-100251 (2017).

[25] **A. L. Pellegrino, M. R. Catalano, P. Cortelletti, G. Lucchini, A. Speghini, G. Malandrino:** Novel sol–gel fabrication of Yb^{3+}/Tm^{3+} co-doped β-$NaYF_4$ thin films and investigation of their upconversion properties. *Photochem. Photobiol. Sci.* **17**, 1239- 1246 (2018).

[26] **S. C. Thompson, D. J. Cole-Hamilton, D. D. Gilliland, M. L. Hitchman, J.C. Barnes**: Stable and volatile β-diketonate complexes of copper, calcium, strontium, barium, and yttrium for use as chemical vapor deposition precursors. *Adv. Mater. Opt. Electron.* **1,** 81-97 (1992).

[27] **G. Malandrino, F. Castelli, I. L. Fragalà**: A novel route to the second-generation alkaline-earth metal precursors for metal-organic chemical vapor deposition: one-step synthesis of M(hfa)$_2$·tetraglyme (M = Ba, Sr, Ca and Hhfa = 1,1,1,5,5,5-hexafluoro-2,4-pentanedione). *Inorg. Chim. Acta* **224**,203-207 (1994).

[28] **G. Malandrino, I. L. Fragalà, D. A. Neumayer, C. L. Stern, B. J. Hinds, T. J. Marks:** Synthesis, characterization and crystal structure of a new thermally stable and volatile precursor [bis(1,1,1,2,

For Peer Review

2,3,3,7,7,8,8,9,9,9-tetradecafluorononane-4,6-dionato)tetraglyme]barium(II) for MOCVD application. *J. Mater. Chem.* **4**, 1061- 1066 (1994).

[29] **G. Malandrino, D. S. Richeson, T. J. Marks, D. C. DeGroot, J. L. Schindler, C. R. Kannewurf:** Phase-selective route to high Tc superconducting thallium barium calcium copper oxide ($Tl_2Ba_2Ca_{n-1}Cu_nO_{2n+4}$) films: combined metalorganic chemical vapor deposition using an improved barium precursor and stoichiometry-controlled thallium vapor diffusion. *Appl. Phys. Lett.* **58**, 182-184 (1991).

[30] **R. D. Shannon**: Revised effective ionic radii and systematic studies of interatomic distances in halides and chalcogenides. *Acta Crystallogr.* **32**, 751– 767 (1976).

[31] **F. A. Cotton, G. Wilkinson, C. A. Murillo, M. Bochmann:** Advanced Inorganic Chemistry. Wiley/Interscience **6th ed**., (1999).

[32] **J. A. Belot, D. A. Neumayer, C. J. Reedy, D. B. Studebaker, B. J. Hinds, C. L. Stern, T. J. Marks:** Volatility by Design. Synthesis and Characterization of Polyether Adducts of Bis(1,1,1,5,5,5-hexafluoro-2,4- pentanedionato)barium and Their Implementation as Metal-Organic Chemical Vapor Deposition Precursors. *Chem. Mater.* **9**, 1638-1648 (1997).

[33] **S. R. Drake, A. Lyons, D. J. Otway, A. M. Z. Slawin, D. J. Williams:** Lanthanide β-diketonate glyme complexes exhibiting unusual co-ordination modes**.** *J. Chem. Soc. Dalton Trans.***15**, 2379-2386 (1993).

[34] **G. Xu, Z.-M. Wang, Z. He, Z. Liu, C.-S. Liao, C.-H. Yan:** Synthesis and Structural Characterization of Nonanuclear Lanthanide Complexes. *Inorg. Chem.* **41**, 6802-6807 (2002).

[35] **G. G. Condorelli, G. Malandrino, I. L. Fragalà**: Engineering of molecular architectures of β-diketonate precursors toward new advanced materials. *Coord. Chem. Rev.* **251**, 1931–1950 (2007).

[36] **G. Malandrino, I. L. Fragalà, P. Scardi:** Heteroepitaxy of $LaAlO_3$ (100) on $SrTiO_3$ (100): In situ growth of LaAlO3 thin films by metal-organic chemical vapor deposition from a liquid single source *Chem. Mater*. **10**, 3765-3768 (1998).

For Peer Review

[37] **N. P. Kuzmina, D. M. Tsymbarenko, I. E. Korsakov, Z. A. Starikova, K. A. Lysenko, O. V. Boytsova, A. V. Mironov, I. P. Malkerova, A. S. Alikhanyan**: Mixed ligand complexes of AEE hexafluoroacetylacetonates with diglyme: Synthesis, crystal structure and thermal behavior. *Polyhedron* **27**, 2811-2818 (2008).

[38] **A. M. Makarevich, P. P. Semyannikov, N. P. Kuzmina:** Saturation Vapor Pressure of the Mixed_Ligand Calcium Bis(hexafluoroacetylacetonate) Complex with Diglyme and Water. *Russian J. Inorg. Chem.* **55**, 1940-1944 (2010).

[39] **A. M. Makarevich, A. S. Shchukin, A. V. Markelov, S. V. Samoilenkov, P. P. Semyannikov, N. P. Kuzmina:** Low-temperature MOCVD of epitaxial CaF_2 and SrF_2 films. *ECS Trans.* **25**, 525-532 (2009).

[40] **S. Fujihara, Y. Kadota and T. Kimura:** Role of Organic Additives in the Sol-Gel Synthesis of Porous CaF_2 Anti-Reflective Coatings. *J. Sol–Gel Sci. Technol.* **24**, 147–154 (2002).

[41] **B. Chen, F. Wang:** Combating Concentration Quenching in Upconversion Nanoparticles. *Accounts Chem. Res.* **53**, 358-367 (2020).

[42] **K. Z. Zheng, K. Y. Loh, Y. Wang, Q. S. Chen, J. Y. Fan, T. Jung, S. H. Nam, Y. D. Suh, X. G. Liu:** Recent advances in upconversion nanocrystals: Expanding the kaleidoscopic toolbox for emerging applications. *Nano Today* **29**, 100797 (2019).

[43] **D. Kang, E. Jeon, S. Kim, J. S. Lee**: Lanthanide-Doped Upconversion Nanomaterials: Recent Advances and Applications. *Biochip J*. **14**, 124-135 (2020).

[44] **A. Baride, G. Sigdel, W. M. Cross, J. J. Kellar, P. S. May:** Near Infrared-to-Near Infrared Upconversion Nanocrystals for Latent Fingerprint Development. *ACS Appl. Nano Mater.* **2**, 4518-4527 (2019).

[45] **D. Kumar, S. K. Sharma, S. Verma, V. Sharma, V. Kumar**: A Short Review on Rare Earth Doped $NaYF_4$ Upconverted Nanomaterials for Solar Cell Applications. *Mater. Today Proc.* **21**, 1868-1874 (2020).

For Peer Review

[46] **J. Day, S. Senthilarasu, T. K. Mallick:** Improving spectral modification for application in solar cells: a review. *Renew Energ.* **132**, 186-205 (2019).

[47] **Q. Z. Zhang, F. Yang, Z. H. Xu, M. Chaker, D. L. Ma:** Are lanthanide-doped upconversion materials good candidates for photocatalysis?. *Nanoscale Horiz.* **4**, 579-591 (2019).

[48] **S. Ullah, E. P. Ferreira-Neto, C. Hazra, R. Parveen, H. D. Rojas-Mantilla, M. L. Calegaro, Y. E. Serge-Correales, U. P. Rodrigues, S. J. L. Ribeiro**: Broad spectrum photocatalytic system based on $BiVO_4$ and $NaYbF_4:Tm^{3+}$ upconversion particles for environmental remediation under UV-vis-NIR illumination. *Appl. Catal. B-Environ.* **243**, 121-135 (2019).

[49] **T. S. Atabaev, A. Molkenova:** Upconversion optical nanomaterials applied for photocatalysis and photovoltaics: Recent advances and perspectives. *Front. Mater. Sci.* **13**, 335-341 (2019).

[50] **D. S. Reig, B. Grauel, V. A. Konyushkin, A. N. Nakladov, P. P. Fedorov, D. Busko, I. A. Howard, B. S. Richards, U. Resch-Genger, S. V. Kuznetsov, A. Turshatov, C. Wurth:** Upconversion properties of $SrF_2:Yb^{3+},Er^{3+}$ single crystals, *J. Mater. Chem. C* **8**, 4093-4101 (2020).

[51] **M. Kraft, C. Wurth, E. Palo, T. Soukka, U. Resch-Genger:** Colour-optimized Quantum Yields of Yb, Tm Co-doped Upconversion Nanocrystals. *Methods Appl. Fluoresc.* **7**, 24001 (2019).

[52] **P. S. May, A. Baride, M. Y. Hossan, M. Berry:** Measuring the internal quantum yield of upconversion luminescence for ytterbium-sensitized upconversion phosphors using the ytterbium(III) emission as an internal standard. *Nanoscale* **10**, 17212-17226 (2018).

For Peer Review

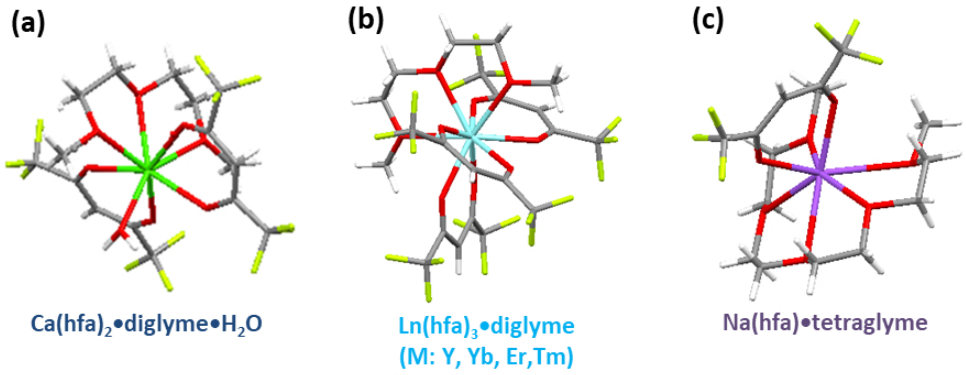

Figure 1. Molecular structures of (a) $Ca(hfa)_2$•diglyme•H_2O, (b) $Ln(hfa)_3$•diglyme and (c) Na(hfa)•tetraglyme (Ln =Y, Yb, Tm, Er) precursors.

153x65mm (150 x 150 DPI)

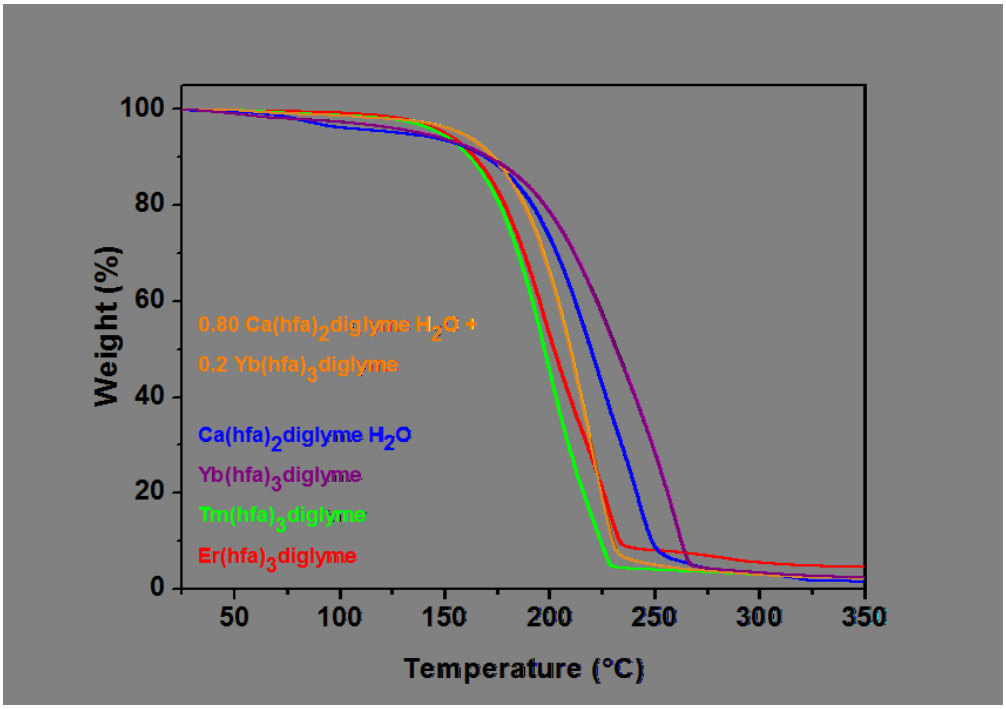

Figure 2. Comparison of thermogravimetric curves of the single precursors, Ca(hfa)sub>2•diglyme•H_2O and $Ln(hfa)_3$•diglyme (Ln = Yb, Er and Tm), and of the Ca(hfa)sub>2•diglyme•H_2O and $Yb(hfa)_3$•diglyme mixture in a Ca : Yb mole ratio of 0.80 : 0.20.

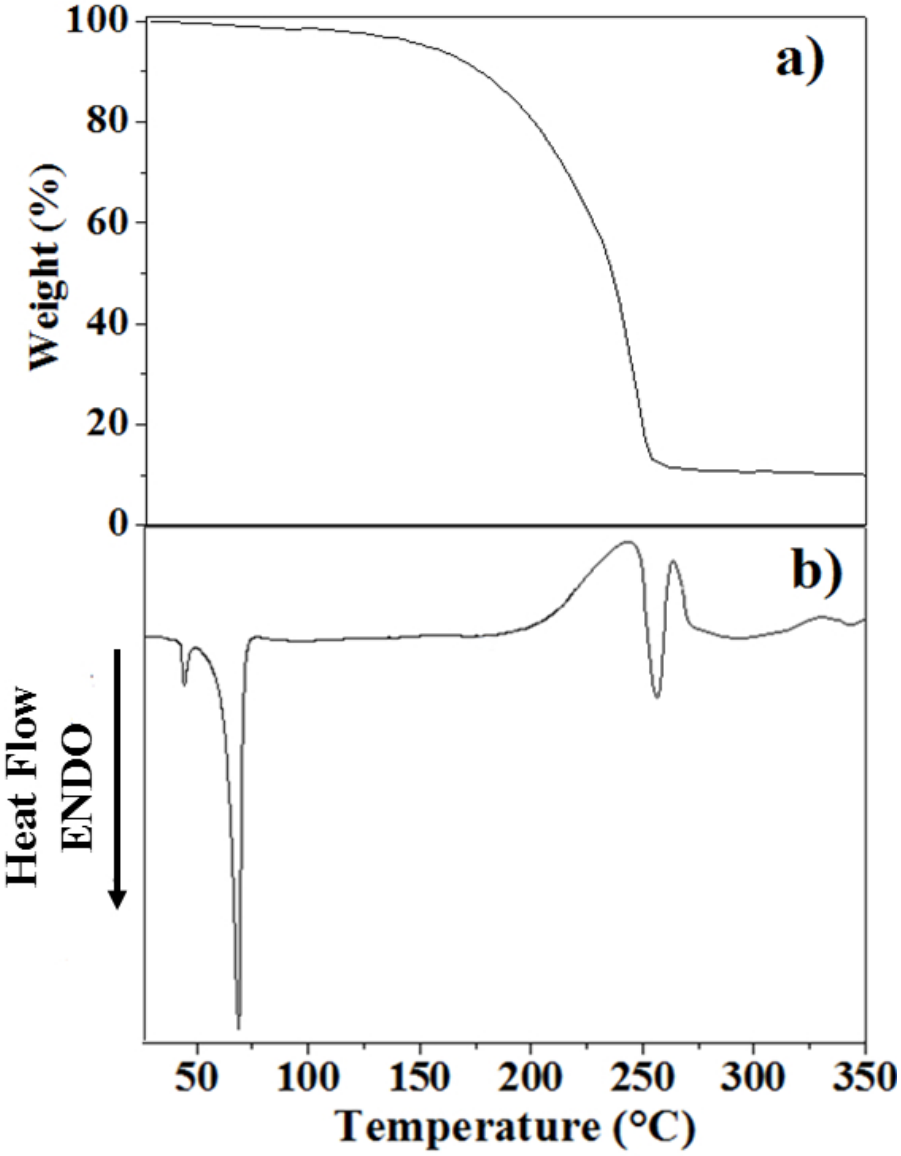

Figure 3. TGA (a) and DSC (b) of the Na(hfa)•tetraglyme adduct.

97x127mm (150 x 150 DPI)

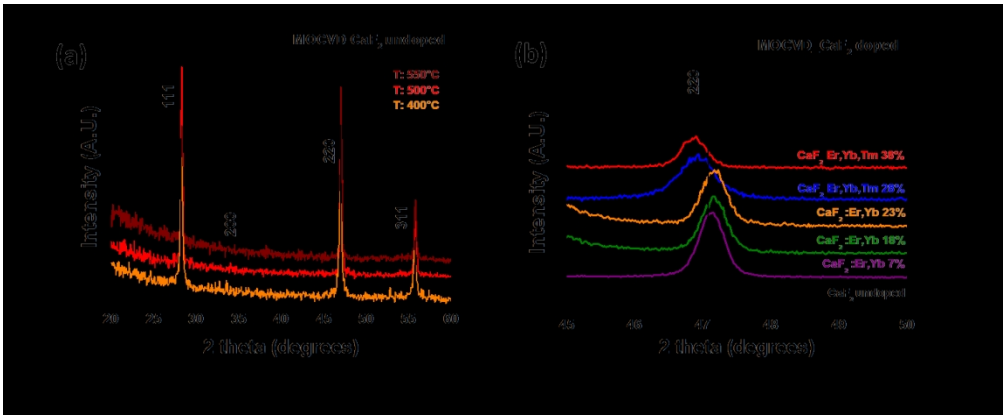

Figure 4. (a) XRD patterns of undoped CaF_2 at different deposition temperatures; and (b) magnification of the 220 reflection of the CaF_2 films doped with different amount of doping ions Yb, Er and Tm (deposition temperature 450°C, substrate Si(100)). The black lines indicate the theoretical positions of the CaF_2 phase peaks.

260x107mm (150 x 150 DPI)

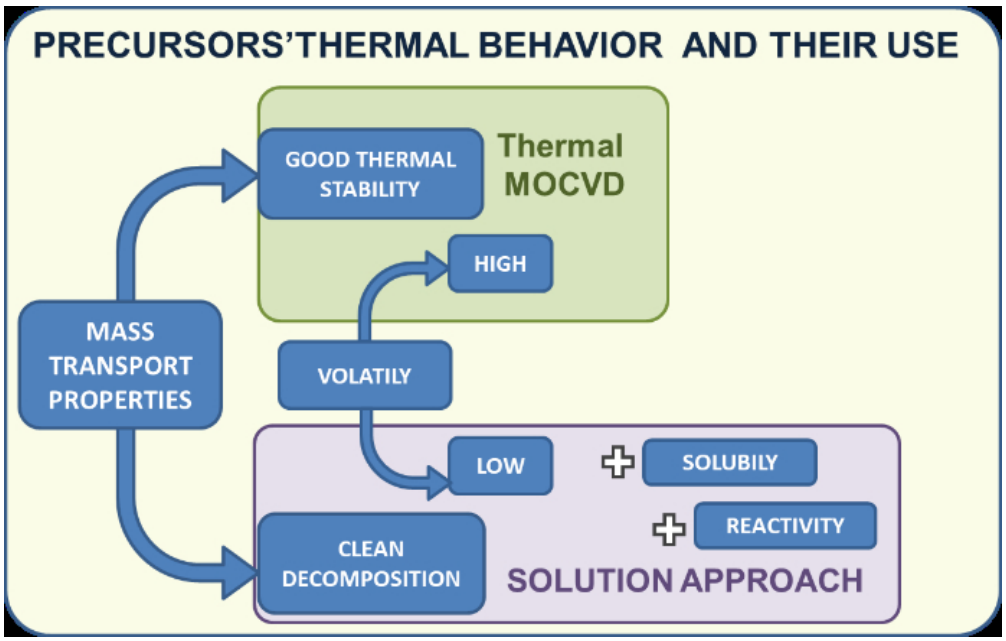

Scheme 1. Precursors' thermal behavior and their properties for application in vapor and solution approaches.

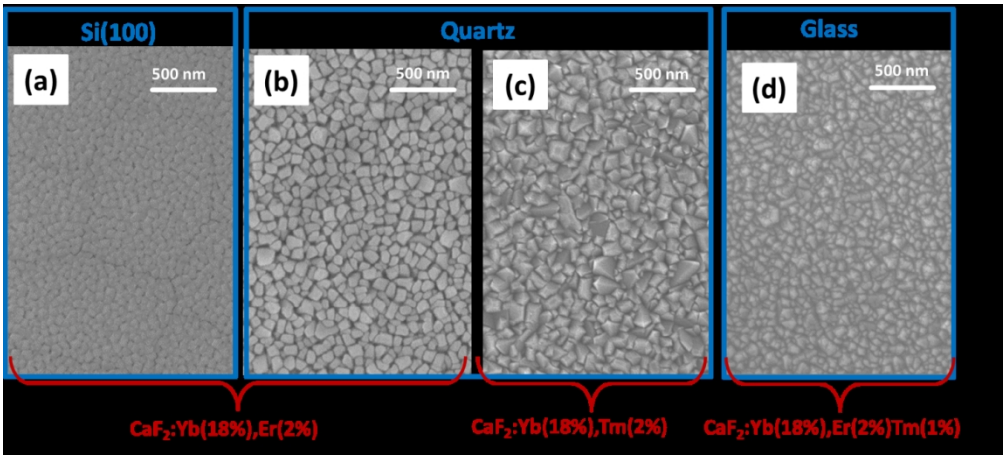

Figure 5. FE-SEM images of CaF_2:Yb^{3+}(18%),Er^{3+}(2%) deposited at 500 °C on (a) Si(100) and (b) quartz. FE-SEM images of (c) CaF_2:Yb^{3+}(18%),Tm^{3+}(2%) deposited at 500 °C on quartz, and (d) CaF_2:Yb^{3+}(18%),Er^{3+}(2%),Tm^{3+}(1%) deposited at 450 °C on glass.

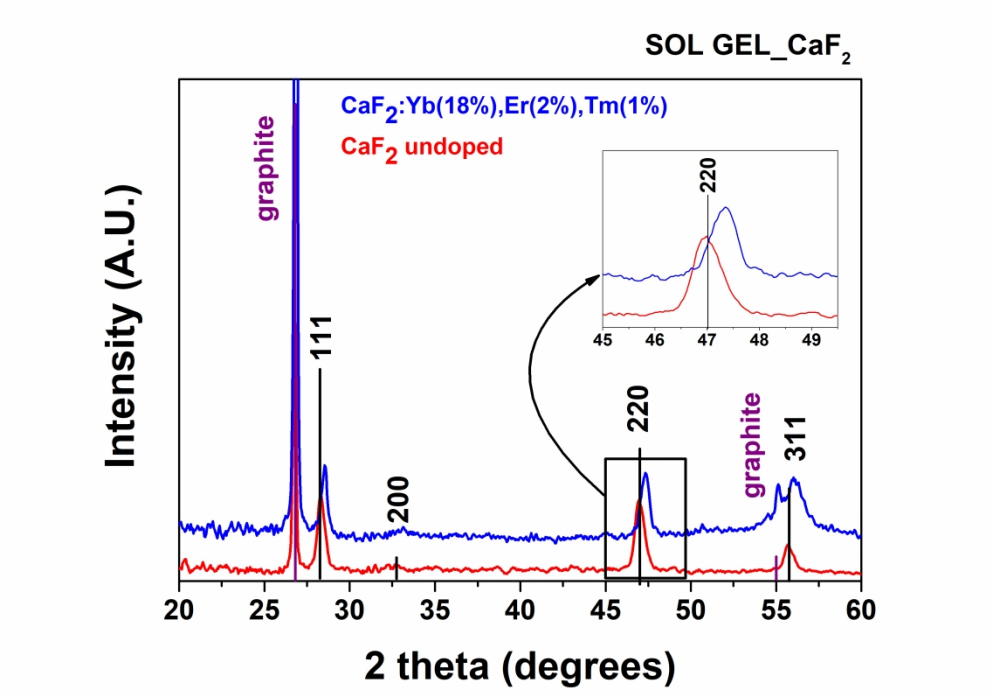

Figure 6. XRD patterns of undoped CaF_2 (red line) and CaF_2:Yb^{3+}(18%),Er^{3+}(2%),Tm^{3+}(1%) (blue line) thin films on Si(100) at annealing temperature of 400 °C (sol-gel/spin-coating method). Graphite is used as an internal standard.

288x201mm (300 x 300 DPI)

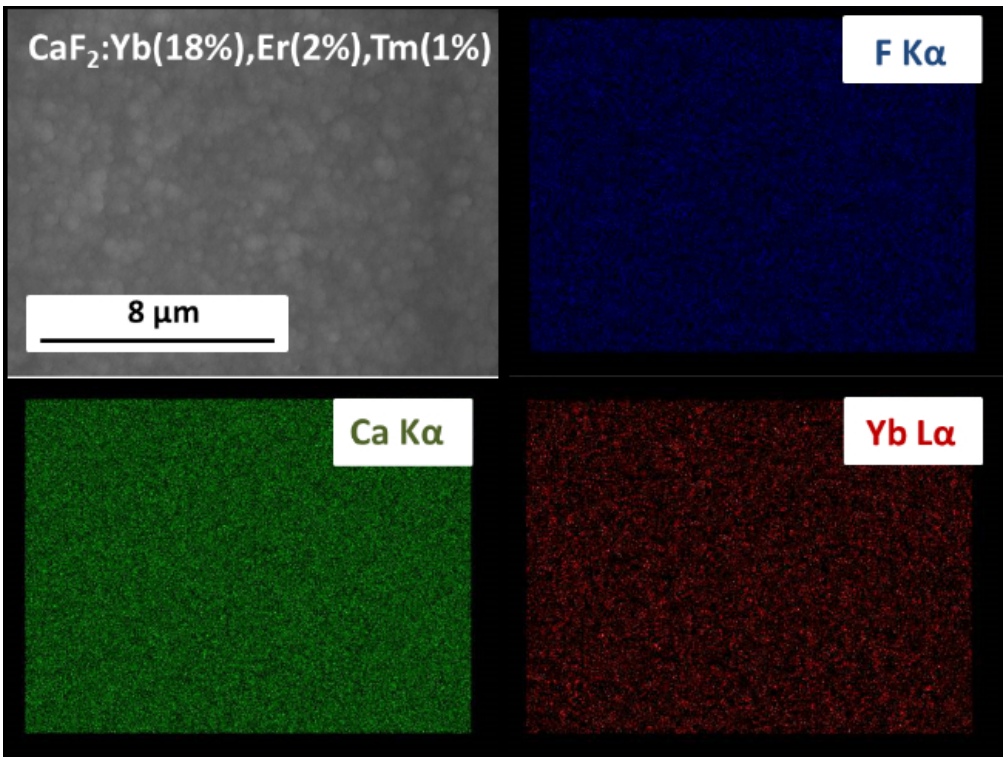

Figure 7. EDX maps analysis of Ca, F and Yb distribution on CaF_2:Yb^{3+}(18%), Er^{3+}(2%), Tm^{3+}(1%) thin films on Si(100).

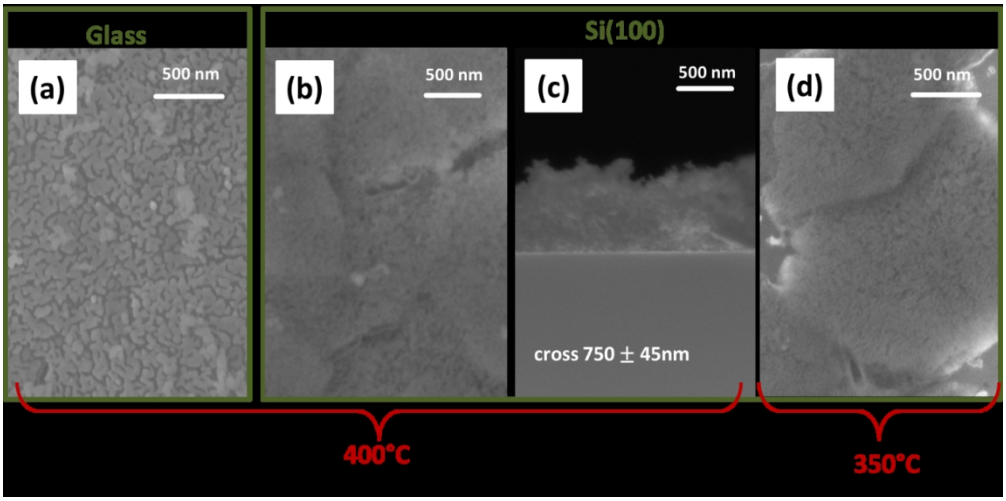

Figure 8. FE-SEM images of (a) undoped CaF2 film deposited at 400 °C on glass. FE-SEM images of CaF_2:Yb^{3+}(18%), Er^{3+}(2%), Tm^{3+}(1%) on Si(100) deposited on Si at (b-c) 400 °C, and (d) 350 °C.

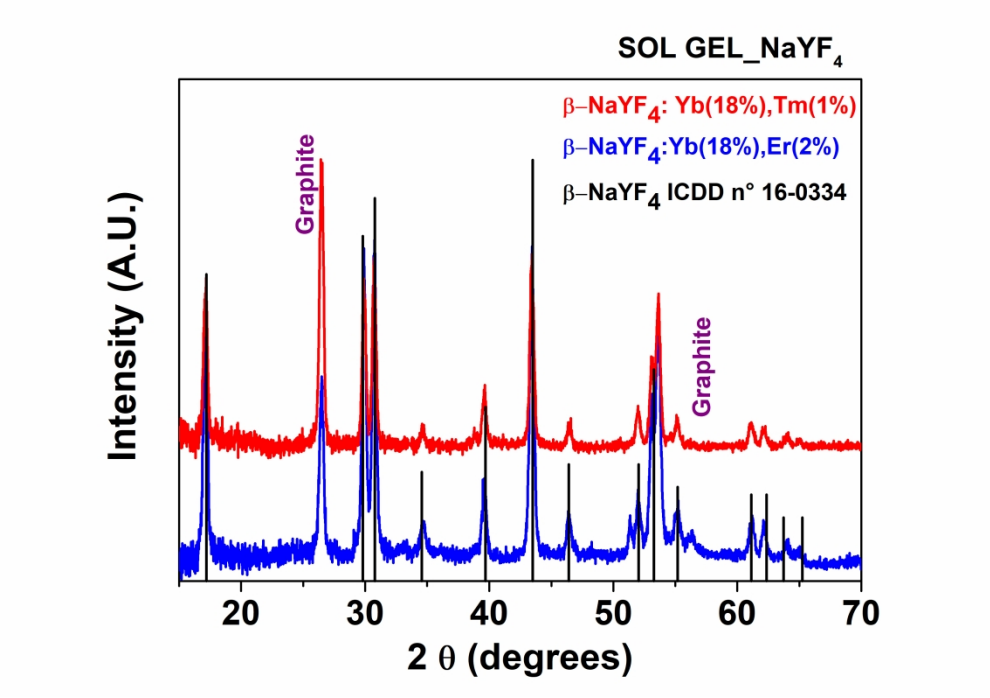

Figure 9. XRD patterns of β-NaYF4:Yb^{3+}(18%),Er^{3+}(2%) (blue line) and β-NaYF4: Yb^{3+}(18%), Tm^{3+}(0.5%) (red line) thin films on Si(100) at annealing temperature of 400°C (sol-gel/spin-coating method).

288x201mm (300 x 300 DPI)

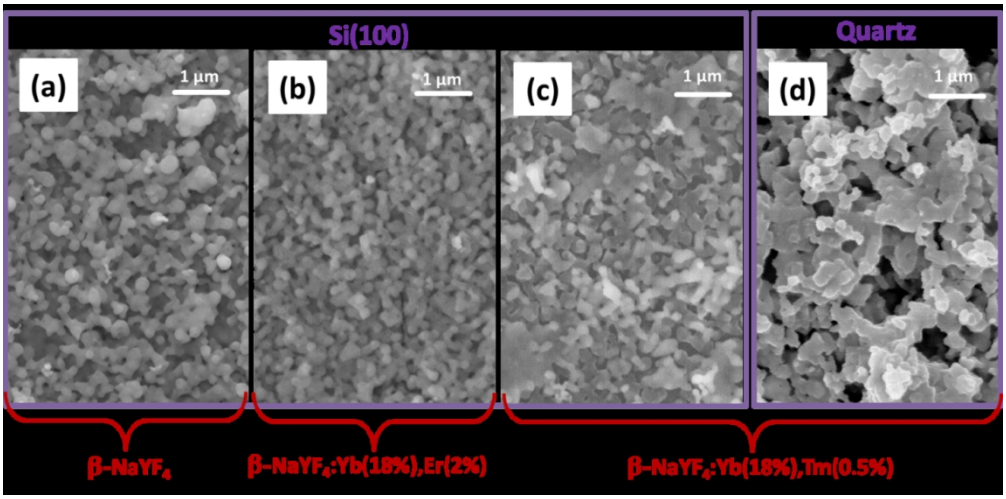

Figure 10. FE-SEM images of undoped β-NaYF4 (a) and β-NaYF4: Yb^{3+}(18%), Er^{3+}(2%) (b) at 400°C on Si(100). β-NaYF4: Yb^{3+}(18%), Tm^{3+}(0.5%) thin films deposited at 400°C on Si(100) (c) and on quartz (d).

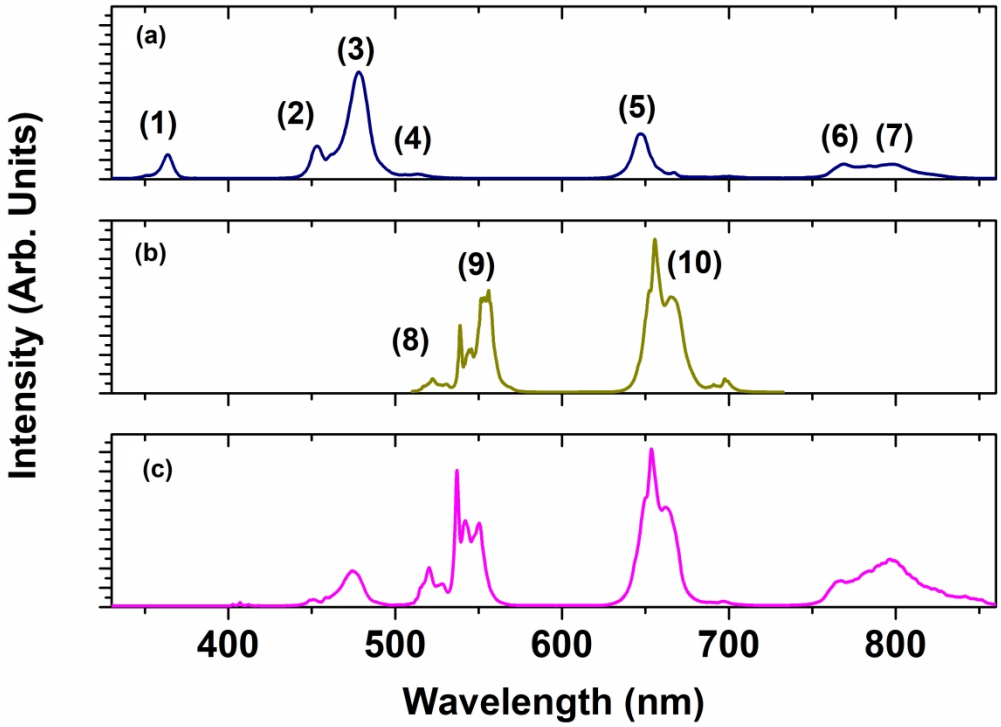

Figure 11. Upconversion spectra of (a) CaF_2: Yb^{3+}(18%), Tm^{3+}(2%) thin film on quartz at 500 °C; (b) CaF_2: Yb^{3+}(18%), Er^{3+}(2%) thin film on quartz at 500 °C; (c) CaF_2: Yb^{3+}(18%), Er^{3+}, Tm^{3+}(1%) thin film deposited by sol-gel technique and annealed at 350 °C.

999x720mm (96 x 96 DPI)

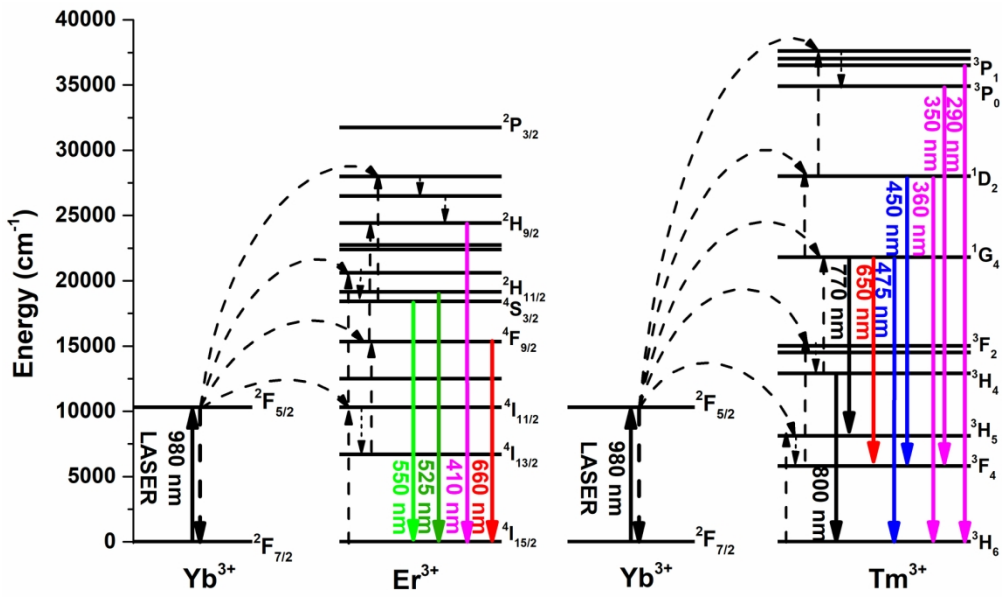

Figure 12. Energy level scheme for radiative and non-radiative processes upon 980 nm laser excitation involving Yb^{3+}, Er^{3+} and Yb^{3+}, Tm^{3+} ions. Solid arrows: radiative transitions. Dashed arrows: energy transfer processes, phonon mediated decays.

79x47mm (600 x 600 DPI)

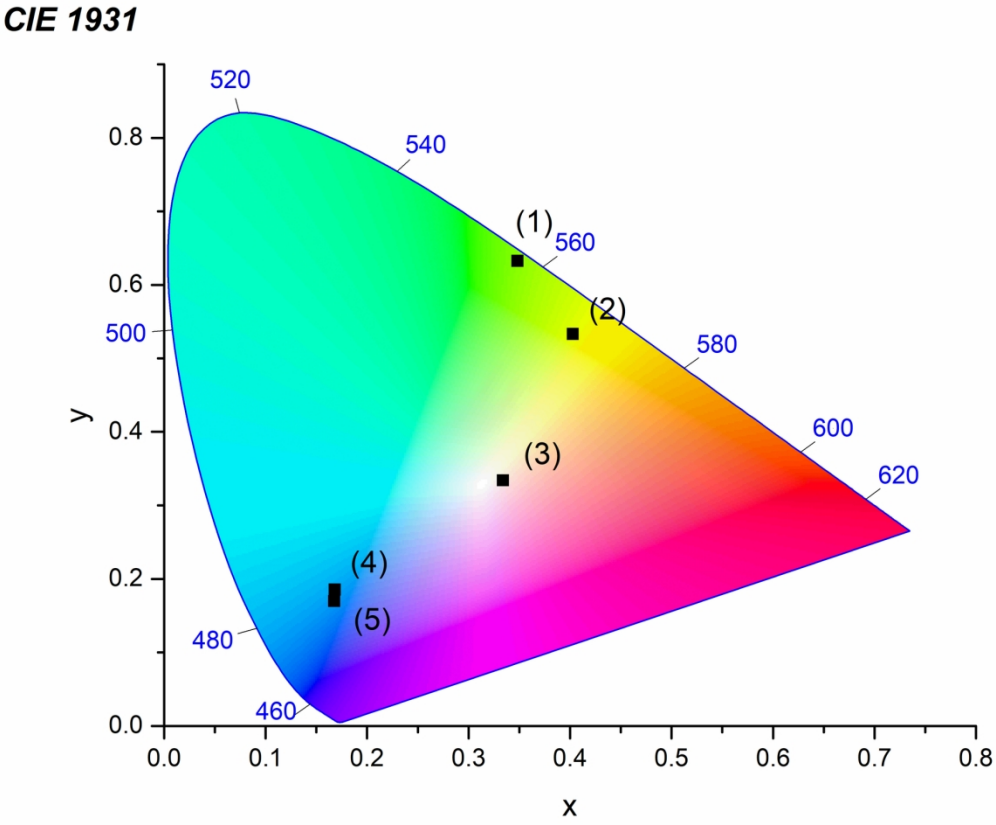

Figure 13. CIE 1931 color coordinates of upconversion upon 980 laser excitation for thin films of: (1) $NaYF_4$: Yb^{3+}(18%), Er^{3+}(2%) prepared by sol-gel technique; (2) CaF_2: Yb^{3+}(18%), Er^{3+}(2%), prepared by MOCVD technique; (3) CaF_2: Yb^{3+}(18%), Er^{3+}(2%), Tm^{3+}(1%) prepared by sol gel technique; (4) CaF_2: Yb^{3+}(18%), Tm^{3+}(2%), single layer prepared by MOCVD technique; (5) $NaYF_4$: Yb^{3+}(18%), Tm^{3+}(0.5%) prepared by sol-gel technique.

79x66mm (600 x 600 DPI)

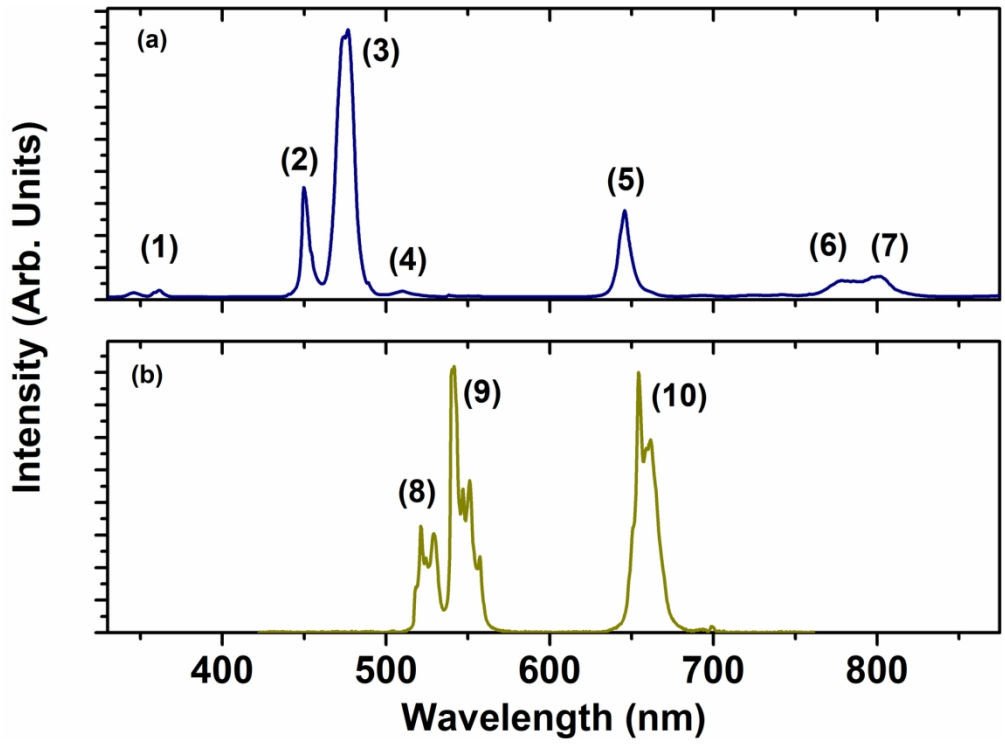

Figure 14. Upconversion spectra upon 980 nm laser excitation (power density of 1 W/cm2) for (a) $NaYF_4$: Yb^{3+}(18%), Tm^{3+}(0.5%) thin film and (b) $NaYF_4$: Yb^{3+}(18%), Er^{3+}(2%) thin film, deposited by sol gel technique.

79x58mm (600 x 600 DPI)

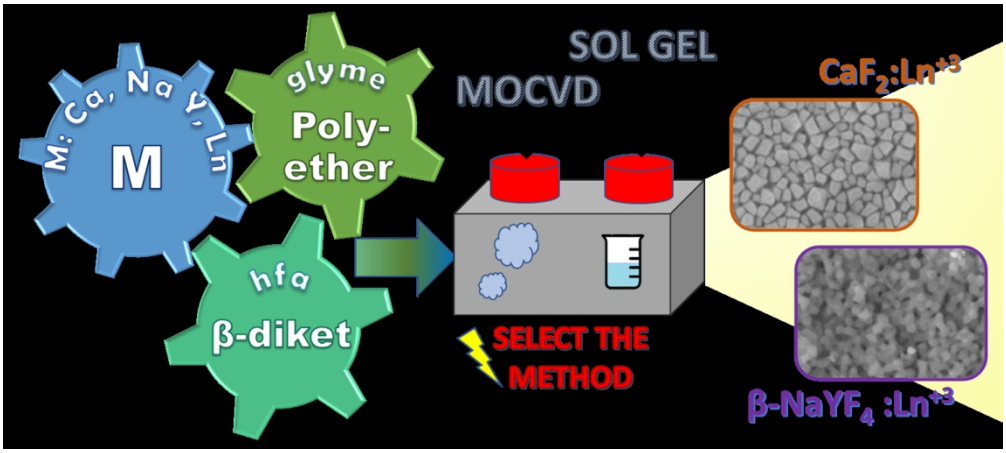

Graphical abstract figure

259x115mm (150 x 150 DPI)